



HAL
open science

A mouse model for monitoring calpain activity under physiological and pathological conditions

Marc Bartoli, Nathalie Bourg, Daniel Stockholm, Fabrice Raynaud, Antony Delevacque, Yang Han, Perrine Borel, Kenza Seddik, Nasser Armande, Isabelle Richard

► To cite this version:

Marc Bartoli, Nathalie Bourg, Daniel Stockholm, Fabrice Raynaud, Antony Delevacque, et al.. A mouse model for monitoring calpain activity under physiological and pathological conditions. *Journal of Biological Chemistry*, 2006, 281 (51), pp.39672-39680. 10.1074/jbc.M608803200 . hal-01610049

HAL Id: hal-01610049

<https://hal.science/hal-01610049>

Submitted on 28 May 2021

HAL is a multi-disciplinary open access archive for the deposit and dissemination of scientific research documents, whether they are published or not. The documents may come from teaching and research institutions in France or abroad, or from public or private research centers.

L'archive ouverte pluridisciplinaire **HAL**, est destinée au dépôt et à la diffusion de documents scientifiques de niveau recherche, publiés ou non, émanant des établissements d'enseignement et de recherche français ou étrangers, des laboratoires publics ou privés.



Distributed under a Creative Commons Attribution 4.0 International License

A Mouse Model for Monitoring Calpain Activity under Physiological and Pathological Conditions*

Received for publication, September 12, 2006; Published, JBC Papers in Press, October 20, 2006; DOI 10.1074/jbc.M608803200

Marc Bartoli^{†1}, Nathalie Bourg^{†1}, Daniel Stockholm^{†1}, Fabrice Raynaud[‡], Antony Delevacque[‡], Yang Han[‡], Perrine Borel[‡], Kenza Seddik[‡], Nasser Armande[‡], and Isabelle Richard^{†2}

From [†]Généthon/CNRS-UMR8115, 1 rue de l'Internationale 91000 Evry, France and [‡]CNRS-UMR5539/Université de Montpellier, Place E. Bataillon, 34000 Montpellier, France

Calpains are Ca²⁺-dependent cysteine proteases known to be important for the regulation of cell functions and which aberrant activation causes cell death in a number of degenerative disorders. To provide a tool for monitoring the status of calpain activity *in vivo* under physiological and pathological conditions, we created a mouse model that expresses ubiquitously a fluorescent reporter consisting of eCFP and eYFP separated by a linker cleavable by the ubiquitous calpains. We named this mouse CAFI for calpain activity monitored by FRET imaging. Our validation studies demonstrated that the level of calpain activity correlates with a decrease in FRET (fluorescence resonance energy transfer) between the two fluorescent proteins. Using this model, we observed a small level of activity after denervation and fasting, a high level of activity during muscle regeneration and ischemia, and local activity in damaged myofibers after exercise. Finally, we crossed the CAFI mouse with the α -sarcoglycan-deficient model, demonstrating an increase of calpain activity at the steady state. Altogether, our results present evidence that CAFI mice could be a valuable tool in which to follow calpain activity at physiological levels and in disease states.

Calpains (EC 3.4.22.17) are Ca²⁺-regulated cytosolic cysteine proteases whose most studied members are the two ubiquitous calpains 1 and 2 (also known as μ - and m-calpains, respectively; for a review see Ref. 1). Through limited proteolysis of their substrates, they were proposed to regulate key cellular functions involving cytoskeleton reorganization such as cell adhesion, cell motility, vesicular trafficking, as well as signal transduction and apoptosis (1). However, several crucial questions on calpain biology remain unanswered. For instance, few clues exist on where and when calpains could be activated in the cell. We also have no clear data on the level of activity of calpains at the steady state.

Inappropriate calpain activation has been implicated in various disease states including traumatic spinal cord and brain injuries, cataract formation, cerebral and heart ischemia,

hypertension, arthritis, Duchenne muscular dystrophy, and neurodegenerative disorders such as Alzheimer disease (2–6). The cell injury in most of these pathologies is initiated by the loss of Ca²⁺ homeostasis, which leads to calpain activation, cleavage of structural and regulatory proteins, and finally to necrotic cell death (7–9). The implication of calpains in these disorders has identified them as important potential therapeutic targets and has raised interest in the use of specific calpain inhibitors as a potent treatment (10–13).

The ability to follow *in vivo* calpain activity is important for physiological, pathological, and therapeutic evaluations. For this purpose, genetically encoded probes that monitor calpain activity have been published in recent years (14, 15). In this report, we generated a mouse model expressing an indicator of calpain activity, based on the fluorescence resonance energy transfer (FRET)³ technique. We named this model CAFI for calpain activity monitored by FRET imaging. After performing validation studies, this model was used to quantify the proteolytic activity of ubiquitous calpains in several biological processes in skeletal muscle. Calpain activity was visualized *in vivo* in exercise-induced damages after denervation, after fasting, during the degeneration and regeneration processes following injury, and during ischemia. We also crossed this model with a model deficient in α -sarcoglycan (16) and demonstrated an elevation of basal calpain activity compared with normal muscle. Our data showed that the CAFI model can be useful for real-time visualization of spatial and temporal activity of calpains under physiological and pathological conditions.

EXPERIMENTAL PROCEDURES

Generation of CAFI and SARCAFI Models—The construction of the reporter cassette was previously described (14). CAFI mice were generated by Speedy Mouse[®] Technology (Nucleis, France) to produce a single copy transgene insertion at the *hprt* locus. The coding sequence of the calpain sensor was excised as a NheI-AflIII fragment and cloned into the EcoRI site of the polylinker of the Gateway[®] pENTR-1A vector (Invitrogen) previously modified to include the ubiquitous cytomegalovirus immediate-early enhancer chicken β -actin hybrid

* This work was funded in part by the Association Française contre les Myopathies, Genopole[®] (Evry) and the Fondation pour la Recherche Médicale. The costs of publication of this article were defrayed in part by the payment of page charges. This article must therefore be hereby marked "advertisement" in accordance with 18 U.S.C. Section 1734 solely to indicate this fact.

[†] These authors contributed equally to this work.

[‡] To whom correspondence should be addressed: Généthon/CNRS-UMR8115, 1 rue de l'Internationale, 91000 Evry, France. Tel.: 33-1-69-47-29-38; Fax: 33-1-60-77-86-98; E-mail: richard@genethon.fr.

³ The abbreviations used are: FRET, fluorescence resonance energy transfer; CAFI, calpain activity monitored by FRET imaging; ES, embryonic stem cell; HAT, hypoxanthine-aminopterin-thymidine; ROI, region of interest; eCFP, enhanced cyan fluorescent protein; eYFP, enhanced yellow fluorescent protein; GFP, green fluorescent protein; FRAP, fluorescence recovery after photobleaching; hprt, hypoxanthine-guanine phosphoribosyl transferase; TA, Tibialis anterior; CP1B, calpain inhibitor peptide.

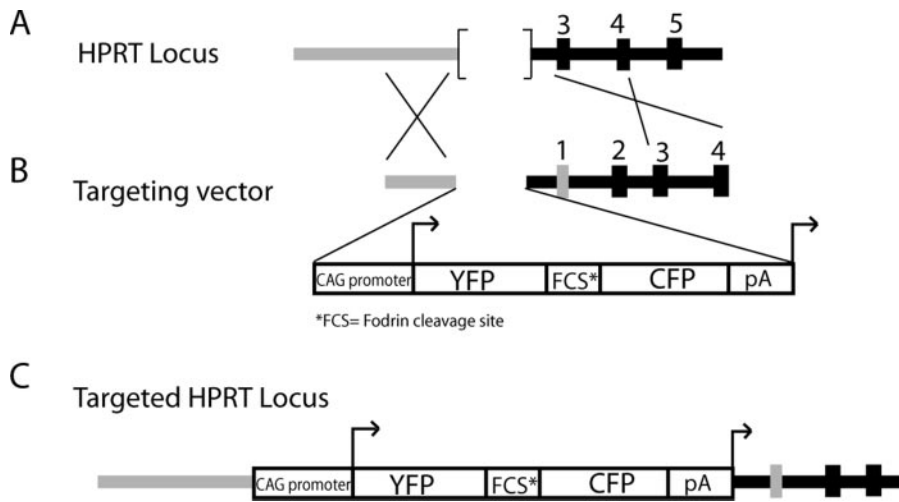


FIGURE 1. Targeted insertion of the calpain sensor at the *hpert* locus. *A*, schematic representation of *hpert* locus of the BPES cells. These cells carry a deletion encompassing exons 1 and 2 of the *hpert* gene. Exons are indicated by boxes. *B*, CAFI construct. The reporter was placed under the control of the CAG promoter and inserted between the 5' and 3' homologous arms targeting the *hpert* locus. *C*, schematic representation of the expected result of homologous recombination. Arrows indicate the transcriptional start sites. A correct homologous recombination restores the *hpert* gene.

(CAG) promoter (17). The transgene was then transferred by the Gateway technology into a destination vector pDEST-HPRT (Nucleis) carrying two homologous arms of the *hpert* gene. The vector was linearized using PvuI and electroporated into *hpert*-deficient BPES-embryonic stem (ES) cells by standard methods. The targeting construct contained the missing sequences in BPES-ES cells and two regions of homology of the *hpert* gene, which allowed insertion of the transgene at this locus (Fig. 1). The targeted ES clones were efficiently selected, thanks to the restoration of the ability to grow in hypoxanthine-aminopterin-thymidine (HAT) medium through a correct homologous recombination. Genotyping of HAT-resistant ES clones was performed by PCR analysis of genomic DNA using a forward primer from the eCFP gene, 181CFP.F 5'-CTCGTGAC-CACCTTCGGCT-3' and a reverse primer from the poly(A) sequence, SV40polyA_45pb.m 5'-GTTTCAGGTTTCAGGGG-GAGG-3'. Samples were amplified for 30 cycles, each consisting of denaturation at 94 °C for 40 s, annealing at 60 °C for 40 s, and elongation at 72 °C for 40 s. Targeted ES cells were injected into C57BL/6-derived blastocysts that were then transplanted into the uteri of recipient females. Resulting chimeric males were bred with C57BL/6 females, and the F1 agouti female offspring were backcrossed with C57BL/6 males. Animals were genotyped by visualization of the fluorescence of the tail sample after YFP excitation.

Hemizygous CAFI females were crossed with *Sgca*-null males (16). Analysis of the progeny was performed by fluorescence examination of the tail sample for the CAFI locus and genotyping with the following primers: KOscgINT1.s 5'-CAGGGCTGGGAGCTGGGTTCTG-3', KOscgEX2.as 5'-CCCAGGGCCTTGATGCCT-3' and KOscgNEOTR.as 5'-GCTATCAGGACATAGCGTTGGCTA-3' for the *Sgca* locus. Using these primers, the *Sgca* wild-type locus gives a band of 1061 bp, and the mutated locus a band of 618 bp. Females that were fluorescent and positive for one *Sgca*-null allele were then crossed with *Sgca*-null males. The progeny was analyzed as stated above to identify the mice

that were homozygous for the *Sgca* mutation while carrying the fluorescent reporter.

In Vivo Experiments—Control mice from the C57BL/6 strain were purchased from Charles River Laboratories (Les Oncins, France). CAFI and SARCAFI mice were produced at our in-house facility. All animal experiments were carried out in agreement with European and national regulations and guidelines.

Mice were subjected to the following different treatments ($n = 3-10$ for each condition). (i) Artificial induction of calpain activation: a solution containing 100 mM CaCl₂, 15 μM ionomycin, 7% fetal calf serum, and 5 mM HEPES (pH 7.4) in a final volume of 50 μl was injected in the muscle. (ii) Fasting: mice were fasted for a 24-h period

with water available *ad libitum*. A subgroup was refed for 6 h before the microscopic examination. (iii) Exercise: mice were forced to run downhill for 1 h at a speed of 10 m/min on a treadmill with a 15° slope. (iv) Degeneration/regeneration of the muscle: 20 μl of notexin (10 μg/ml) were injected in the left TA muscle. (v) Chronic denervation of the muscle: this condition was obtained by cutting the sciatic nerve as described (18). (vi) Ischemia of the muscle: after dissection, the femoral artery was ligatured with Mersilk braided non-absorbable silk (Ethicon).

At the time of examination, mice were anesthetized by intraperitoneal injection of ketamin (100 mg/kg) and xylazin (10 mg/kg). A glass coverslide was positioned on the exposed muscle, and mice were placed on the microscope for direct observation.

Fluorescence and FRET Imaging—FRET microscopy set-up was previously described (14). Laser scanning confocal images were collected on a Bio-Rad confocal microscope system. Analysis was performed in ImageJ with custom-made software named FRET Compute Environment. The software (freely available upon request) implemented as an ImageJ plug-in is designed in four modules that can be used independently or successively through a graphical user interface. The first module converts the images acquired by the LaserSharp software into tiff files. The second module enables the calculation of spectral bleed-through coefficients. The third module calculates the FRET efficiency (FRET_{eff}) and stores the results in float images (32 bits) and in RG images, consisting of a superimposition of the donor (eCFP) channel in green and FRET channel in red. The last module permits the creation of pseudocolor images, giving a comprehensive interpretation of FRET_{eff} calculations. To obtain such images, the float images were first converted in an 8-bit pseudocolor image using a classic rainbow look-up table (red for minimum values, green for middle, and blue for high values). Donor channel pixels below a minimum threshold (50) or higher than a maximum threshold (200) are

Calpain Activity followed by FRET in Model Mice

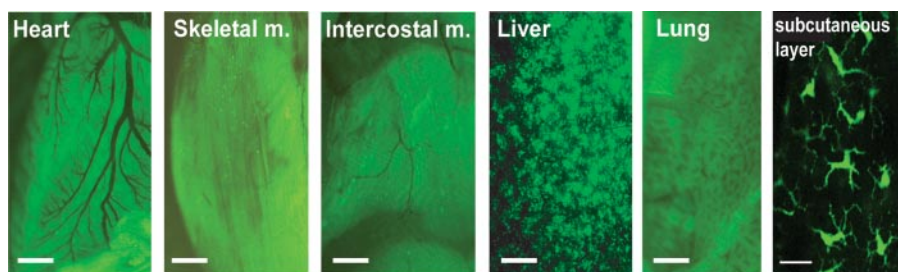


FIGURE 2. Expression of the calpain sensor in living organs. Two-photon images in the CFP filter of cardiac, skeletal, and intercostal muscles, liver, lung, and subcutaneous layer. Scale bars: 1 mm except for subcutaneous layer 20 μ m.

represented in gray scale in the pseudocolor images. The mean FRET efficiency was calculated on the region of interest (ROI) either selected inside fibers or corresponding to the complete image, when there was homogeneity of FRET efficiency.

The calculation of FRET_{eff} in this plug-in takes into account G , a factor that relates the quenching of donor emission due to FRET, to the sensitized emission of the acceptor (19). To determine G experimentally, we expressed a CFP-YFP tandem for which the FRET_{eff} was previously established by fluorescence lifetime imaging microscopy.⁴ We obtained a G value with a mean of 1.7 ± 0.1 after the analysis of various ROIs of muscles fibers expressing the eCFP-eYFP tandem ($n = 3$ independent experiments).

For FRAP experiments, a Leica TCS SP2 confocal microscope (Leica, Mannheim, Germany) was used. Eight bleaching pulses at an excitation of 514-nm wavelength with 100% intensity of an argon laser were initiated at time 0 using a $\times 20$ microscope objective lens. The recovery of fluorescence following the bleach was monitored every 5 s for 3 min and collected through the FRAP module of the Leica software.

Western Blot—For the *in vitro* analysis, organs were cut in three equivalent pieces. One-third was put in lysis buffer (Tris-HCl, 20 mM pH 7.5, NaCl 150 mM, 1% Triton) supplemented with 5 mM EDTA, Complete Mini Protease Inhibitor mixture (Roche Applied Science) and 2 μ M E64 (Sigma) and immediately pulverized. These samples were used as a control. The second third was put in lysis buffer supplemented with 2 mM CaCl₂ for activation, and the last third was put in lysis buffer supplemented with 2 mM CaCl₂ plus 100 μ M MDL28170 (Sigma) and 50 or 100 μ M of calpain inhibitor peptide (CP1B, C9181, Sigma). The two last samples were incubated for 30 min at 37 °C before pulverization. 10 μ g of samples were then processed for Western blotting using a rabbit polyclonal antibody against GFP (Abcam, AB6556–25, dilution 1:5,000) according to standard procedures.

For analysis of the cleavage of the reporter, muscles were quick-frozen in liquid nitrogen, pulverized with UltraTurrax, and rapidly solubilized in Tris-HCl, 20 mM, pH 7.5, NaCl, 150 mM, 2 mM EGTA, 1% Triton containing the Complete Miniprotease Inhibitor mixture and 2 μ M E64. After centrifugation at $8,000 \times g$ for 5 min at +4 °C, the supernatants were mixed with 1 mM dithiothreitol and 1 \times LDS NuPAGE Buffer (Invitrogen) before they were denaturated at 70 °C for 10 min and processed for Western blot as above.

⁴ Dr. Marc Tramier, personal communication.

Detection of Evans Blue-positive Fibers and Immunofluorescence—SARCAFI mice were injected intraperitoneally with Evans blue dye (1 mg/g of body weight). The following day, mice were sacrificed, and muscles were quickly frozen in liquid nitrogen-cooled isopentane. Cryosections (10- μ m thickness) were prepared from frozen muscles. Evans blue-positive fibers were revealed by fluorescence excitation

at 633 nm. Transverse sections were processed for hematoxylin and eosin staining. Immunohistochemical detection of MHCd was performed according to standard procedures with the primary antibody NCL-MHCd (Novocastra).

Statistical Analysis—To determine whether the FRET_{eff} differed between treated and corresponding controls, statistical analyses were performed using the nonparametric Mann-Whitney test, corrected for ties.

RESULTS

Production and Characterization of Mice Expressing the Calpain Sensor—The FRET calpain reporter used in this study (calpain sensor) codes for a fusion protein consisting of eYFP, a cleavage site of α -fodrin, and eCFP. We previously validated by gene transfer experiments the use of this reporter as an effective tool to detect the proteolytic activity of ubiquitous calpains in living mice (14). A mouse model carrying a single copy of this reporter at the hypoxanthine-guanine phosphoribosyl transferase (*hprt*) locus was generated by the Speedy Mouse[®] technology. After construction of the targeting vector, electroporation into BPES-ES cells and selection on HAT medium, three resistant clones were injected into C57BL/6 blastocysts and implanted in recipient females. Two of them gave nine chimeric males with about 100% chimerism. These founders were crossed with C57BL/6 mice, and experiments were conducted in F1-F4 male progeny.

CAFI mice produce litters of normal size and sex ratio and have the expected longevity. Histological examination of tissues revealed no discernable phenotype associated with the expression of the sensor. As expected, a robust fluorescence was detected by direct microscopic examination in selected organs (Fig. 2). In accordance with the fluorescence level, a Western blot performed using an anti-GFP polyclonal antibody gave a strong response in these tissues (data not shown). These analyses showed that the reporter is highly expressed in our model and gave fluorescence sufficiently strong for high resolution *in vivo* imaging.

Considering the level of calpain activity in the context of muscular dystrophies and given the easy access to muscle for experimentation, we focused our attention on muscle tissue. A lower limb was sectioned transversally as a whole, confirming the general distribution of the fluorescence (Fig. 3A). Fluorescence was detected throughout all the myofibers, including the nuclear compartment, without any aggregates being identified (Fig. 3B). It must be noted that in our microscopic set-up, no autofluorescence was detected in normal muscles (data not

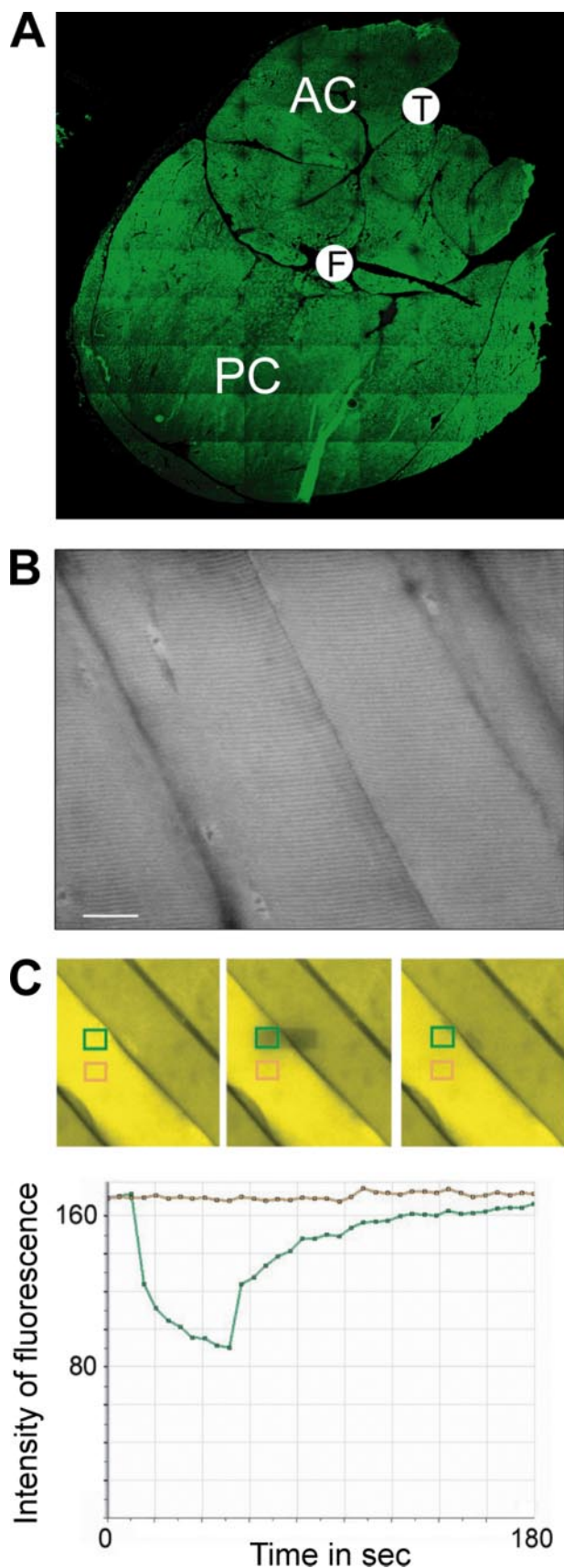


FIGURE 3. *A*, cross section of the lower part of a CAFI hind limb. All muscles in this section appear fluorescent. *AC*, anterior compartment; *PC*, posterior compartment; *T*, tibial bone; *F*, fibula bone. *B*, two-photon image in CFP filter of skeletal muscles showing an evenly distribution of fluorescence between

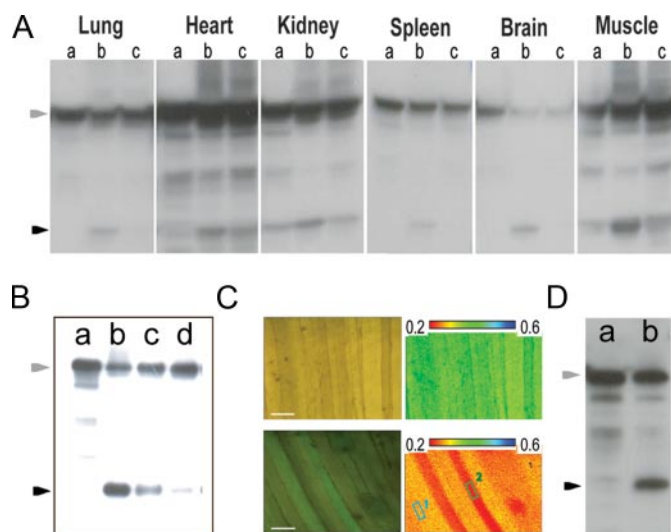


FIGURE 4. *A*, *in vitro* validation of the reporter cleavage in the absence of Ca^{2+} (lane *a*) or in its presence (lanes *b* and *c*) and with (lane *c*) or without (lane *b*) calpain inhibitor. The reporter from muscle extract was revealed with an anti-GFP antibody. Incubation with Ca^{2+} induced a cleavage of the reporter that is prevented by the use of MDL28170. *B*, a similar experiment to *A* was performed using the CP1B peptide. Lane *a* shows the untreated muscle and the other lanes the Ca^{2+} -treated muscles in the presence of the CP1B peptide at a concentration of $0 \mu\text{M}$ (lane *b*), $10 \mu\text{M}$ (lane *c*), and $50 \mu\text{M}$ (lane *d*). *C*, left panels: RG images of CAFI muscle. Right panels: pseudocolor images of FRET_{eff} . The pseudocolor scale is indicated below the images. Upper panels: FRET_{eff} in skeletal muscle at steady state. The mean FRET_{eff} was calculated to be 0.380. Lower panels: FRET_{eff} after Ca^{2+} /ionomycin injection in skeletal muscle. The mean FRET_{eff} for two independent ROI is shown. ROI1 = 0.267 and ROI2 = 0.203; Scale bars: $100 \mu\text{m}$. *D*, an anti-GFP Western blot of the corresponding muscles shows the absence of cleavage of the reporter at the steady state and a cleaved band after Ca^{2+} /ionomycin injection. Gray arrowheads indicate the position of the non-cleaved reporter. Black arrowheads indicate the position of the cleaved reporter.

shown). As occasionally a sarcomeric pattern could be observed, we performed a one-photon fluorescence recovery after photobleaching (FRAP) experiment to determine whether any of the reporter molecules was bound to the sarcomere. A restoration calculated to be 99% of the initial fluorescence was observed within 1 min, indicating that the molecules are freely diffusible and that they would be therefore readily accessible to calpains wherever localized (Fig. 3C). A similar sarcomeric pattern can be seen with other reporters and should correspond to a negative image of the Z disc, a dense protein network of the sarcomere.

Validation of the Reporter Functionality—After sampling, pulverized powder of different tissues was incubated *in vitro* in the presence of Ca^{2+} for 30 min at 37°C in the presence or absence of MDL28170, a potent inhibitor of the ubiquitous calpains. Subsequent analysis of these samples by anti-GFP Western blotting allowed the visualization of the extent of the reporter cleavage. On control samples, no cleavage was evidenced with the exception of the kidney (Fig. 4A, lane *a*). In this tissue, an elevated activity was later confirmed by FRET analysis (data not shown). Because this organ was sampled before others

fibers and diffusion both in the cytoplasmic and nuclear compartments. Scale bar: $100 \mu\text{m}$. *C*, FRAP experiment in skeletal muscle. Upper panels, two-photon image of skeletal muscle before, immediately after, and 2 min after bleaching. Lower panel, normalized plot of fluorescence recovery versus time. The percentage of the mobile fraction was calculated to be 99%.

Calpain Activity followed by FRET in Model Mice

where no activity was observed, we can exclude an artifactual activation because of the treatment. Therefore, it seems to indicate that the ubiquitous calpains are activated in physiological condition in this tissue. Even so, in all the tissues, incubation in the presence of Ca^{2+} led to a cleavage that was inhibited in the presence of MDL28170 (Fig. 4A, lanes b and c). To confirm the specificity of the reporter, we performed a similar experiment using a calpain inhibitor derived from calpastatin, the CP1B peptide (20). Inhibition of cleavage was obtained in a dose-dependent manner in the muscle tissue (Fig. 4B). Hence, we concluded that the reporter expressed in the CAFI model was readily and specifically cleavable by the ubiquitous calpains.

We analyzed the FRET efficiency (FRET_{eff}) in muscle at rest by two-photon confocal microscopy according to the method described under "Experimental Procedures." A homogeneous FRET_{eff} was observed between and among the fibers with a mean of 0.380 (Fig. 4C, upper panels). Then, we performed an intramuscular injection of Ca^{2+} /ionomycin, a condition previously shown to induce calpain activation. Various FRET_{eff} decreases were observed among the fibers, shown by the calculation of the FRET_{eff} in ROI ($\text{ROI1} = 0.267$ and $\text{ROI2} = 0.203$; Fig. 4C, lower panels). A Western blot showed that about 40% of the reporter was effectively cleaved, consistent with the decrease of FRET_{eff} (Fig. 4D). It is noted that when mice died during the experiment, a postmortem cleavage of the reporter was seen associated with a high decrease of FRET_{eff} stressing the importance of *in vivo* analysis when looking for physiological calpain activity.

In Vivo Analysis of Calpain Activity—We analyzed calpain activity by monitoring the muscle of a living animal under various conditions where ubiquitous calpains are known to be up-regulated or activated (21–27).

We set up two different protocols to induce atrophy of the muscle, either by fasting or by denervation. For the fasting experiment, CAFI mice were divided into three experimental groups: a control group, a group where the mice fasted for a 24-h period, and a group where the mice were refed for 6 h after the fasting period. The mean loss of weight after 24-h fasting was 16%, and the mice in the third group recovered half of the lost weight after the refeeding period. A small but statistically significant decrease of 3.6% in FRET_{eff} was observed for both groups that underwent fasting compared with control (Table 1 and Fig. 5, panel a). For the denervation experiment, a chronic cut of the sciatic nerve was performed, and the mice were examined 4 and 14 days after the section. A change of 4.3 and 6.1% in FRET_{eff} was observed at days 4 and 14, respectively (Table 1 and Fig. 5, panel b).

Another protocol was performed where the mice were forced to run on a treadmill for 1 h. Muscles were observed immediately afterward and after a 24-h period. At both periods, a global 10% FRET_{eff} decrease was detected (Table 1 and Fig. 5, panel c). In addition, we observed the appearance of structural anomalies in some fibers. Different phenotypes observed during this protocol are presented in Fig. 6. Most of the time, these disruptions of architecture present as a plugged density associated with a major FRET_{eff} decrease only at one side of the anomaly (black and white arrowheads in Figs. 5, panel c and 6).

TABLE 1
Mean $\text{FRET}_{\text{eff}} \pm \text{S.D.}$ for the number of ROI are presented for different *in vivo* protocols

The percent difference between experiments and controls is also displayed (% Diff.). Significant differences between groups are calculated with the Mann-Whitney algorithm. (A significant difference corresponds to a *p* value < 0.01).

	Fasting			Denervation			Exercise			Notetxin			Ischemia		
	$\text{FRET}_{\text{eff}} \pm \text{S.D.}$	% Diff.	<i>P</i>	$\text{FRET}_{\text{eff}} \pm \text{S.D.}$	% Diff.	<i>P</i>	$\text{FRET}_{\text{eff}} \pm \text{S.D.}$	% Diff.	<i>P</i>	$\text{FRET}_{\text{eff}} \pm \text{S.D.}$	% Diff.	<i>P</i>	$\text{FRET}_{\text{eff}} \pm \text{S.D.}$	% Diff.	<i>P</i>
Control <i>n</i> = 39	0.383 ± 0.0073	–	–	Control <i>n</i> = 32	0.393 ± 0.0043	–	Control <i>n</i> = 33	0.382 ± 0.0035	–	Control <i>n</i> = 29	0.372 ± 0.0102	–	Control <i>n</i> = 60	0.396 ± 0.0235	–
Fasting <i>n</i> = 39	0.369 ± 0.0097	–3.66	<0.001	D4 post-Den. <i>n</i> = 40	0.376 ± 0.0047	–4.33	0h post-ex <i>n</i> = 46	0.342 ± 0.0248	–10.42	D4 post-Not. <i>n</i> = 32	0.255 ± 0.0256	–31.45	Ischemia <i>n</i> = 64	0.293 ± 0.0272	–26.0
Refed <i>n</i> = 65	0.369 ± 0.0057	–3.66	<0.001	D14 post-Den. <i>n</i> = 25	0.369 ± 0.0023	–6.11	24h post-ex. <i>n</i> = 49	0.354 ± 0.0076	–7.33	D7 post-Not. <i>n</i> = 14	0.294 ± 0.0070	–20.97	D9 post-Not. <i>n</i> = 16	0.366 ± 0.0080	–1.61
															0.327

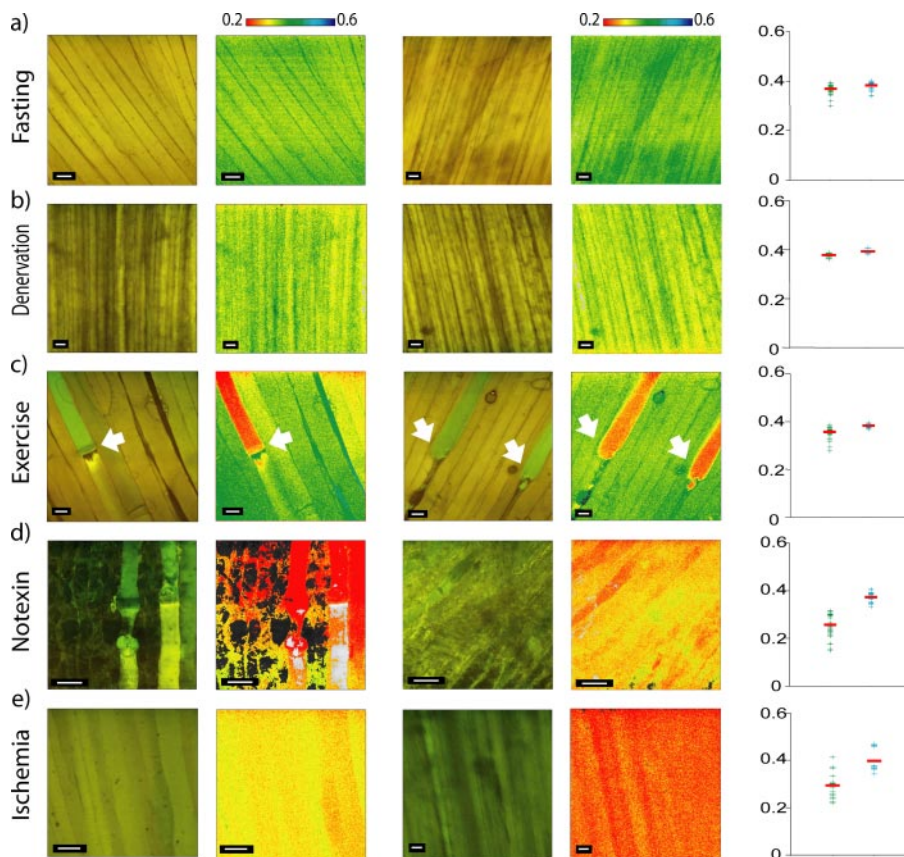


FIGURE 5. *In vivo* activity of the ubiquitous calpains during various conditions. Four left panels, two sets of RG and FRET_{eff} pseudocolor images of skeletal muscle that are representative of the results obtained under different conditions: panel a, 24-h fasting; panel b, 4 days after sciatic nerve section; panel c, 24 h after 1 h long exercise; panel d, 4 days after notexin injection (left panels), 7 days after notexin injection (right panels); panel e, 45 min of ischemia (left panels), 115 min of ischemia (right panels). Graphs on the right display the FRET_{eff} for the different ROI analyzed, in green for the experiment and in blue for the corresponding control. The mean for each condition is shown with a red bar. White arrowheads pointed to structural anomalies observed after exercise with the FRET_{eff} decrease appearing only in one side of the fibers. A large decrease in FRET_{eff} is clearly visible after notexin treatment and ischemia. Scale bars: 40 μm.

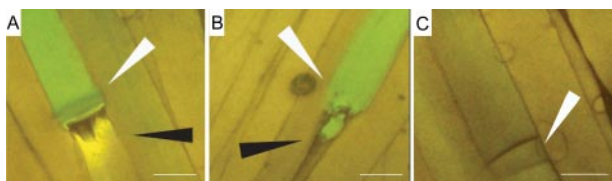


FIGURE 6. RG images of TA muscles obtained after an extensive exercise protocol. White arrowheads point at the anomalies occurring in this condition. A, black arrowhead shows the side where no FRET_{eff} decrease was detected. B, black arrowhead indicates the side where half a fiber disintegrated. C, an example where the FRET_{eff} is similar at both sides of the anomaly. Scale bar: 40 μm.

Calpain activity was also followed up during degeneration and regeneration after notexin injury. Tibialis anterior (TA) muscles were examined 2, 3, 4, 7, and 9 days after injury. From day 0 to day 4, muscles were totally disorganized with fiber necrosis and infiltrates of mononucleated cells. At this stage, large black regions indicated loss of the fluorescence, probably corresponding to necrotic fibers (Fig. 5, panel d). In the remaining fibers, a massive loss of FRET_{eff} occurred as shown by the solid red regions. In the following days, small regenerating myofibers appeared while mononucleated cells disappeared. At day 4, the mean FRET_{eff} for treated samples showed a 31%

decrease (Table 1 and Fig. 5, panel d). At day 7, the mean FRET_{eff} was still low, and at day 9, the FRET_{eff} had returned to a normal level with an apparently healthy muscle with remaining central nuclei (Table 1 and data not shown).

Finally, we performed a kinetic analysis over 2 h of calpain activity during ischemia. We examined the consequence on the TA muscle after blockade of the blood flow with a femoral clamp. A decrease in FRET_{eff} was noticed as soon as 45 min of ischemia (Table 1 and Fig. 5, panel e). A complete loss of FRET_{eff} occurred after 130 min (data not shown). This loss of FRET_{eff} was very homogeneous among the studied muscle with no apparent damage seen in the myofibers.

*Crossing of CAFI Mice with a Model of Muscular Dystrophy—*An activation of the ubiquitous calpains, secondary to an increase in Ca²⁺ influx through leaky membranes, has been previously reported in the dystrophin-deficient *mdx* mice (2, 7). Disruption of Ca²⁺ homeostasis was also shown in the case of the BIO14.6 hamster deficient in δ-sarcoglycan, a member of the dystrophin-glycoprotein complex (DGC) (28). These observations suggest that excess calpain

activity would constitute a common pathophysiological mechanism in these DGC-related diseases. To analyze *in vivo* calpain activity in the context of muscular dystrophies, we crossed the CAFI model with a model deficient in α-sarcoglycan (*Sgca*-null mice). We named this model SARCAFI. The *Sgca*-null model was chosen instead of *mdx*, because the distance separating the dystrophin gene and the *hprt* locus on chromosome X (15 centiMorgan according to the Mouse Genome Data base) would render difficult the creation of a double model. Offspring were selected according to the fluorescence and genotyping at the *Sgca* locus and were obtained with the expected transmission ratio. SARCAFI mice present the same phenotype as *Sgca*-null mice with lordosis, muscular pseudohypertrophy, and clusters of necrotic and regenerating fibers at the histological level.

We verified that the calpain sensor was expressed in various organs and that it retained its reporter properties by examining mice at 4 weeks of age (data not shown). However, we observed a low level or a lack of expression in some myofibers (Fig. 7A). This observation together with the results from the Evans blue assay and developmental myosin heavy chain (MHCd) immunostaining seem to indicate that this low expression could be both related to necrosis and to immaturity of the fibers (data not shown). For the fibers that have a detectable level of expres-

Calpain Activity followed by FRET in Model Mice

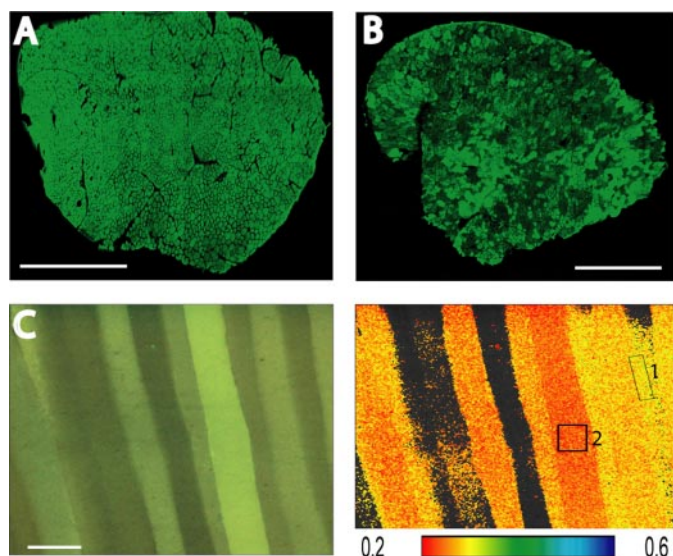


FIGURE 7. *A* and *B*, YFP fluorescence in CAFI anterior compartment (TA + extensor digitorum longus) and SARCAFI TA muscle in 1-month-old mice. The SARCAFI muscle (*B*) showed a mosaic pattern of fluorescence, which differs from the homogeneous distribution obtained with the CAFI muscle (scale bars: 1 mm) (*A*). *C*, left panel: RG image of SARCAFI muscle. Not all fibers are fluorescent as observed in the cross section. Right panel, FRET_{eff} pseudocolor image of skeletal muscle in SARCAFI mice at steady state. The FRET_{eff} was calculated in two different ROIs (ROI1: 0.294; ROI2: 0.237). Those results indicated an activation of ubiquitous calpains in the absence of the α -sarcoglycan protein. Scale bar: 60 μ m.

sion, the FRET_{eff} was 36% lower than in CAFI mice (mean FRET_{eff} = 0.245 \pm 0.02; p < 0.001), reflecting an elevated basal activity of calpain in dystrophic muscles (Fig. 7*B*).

DISCUSSION

In this report, we generated a model that ubiquitously expressed a fluorescent reporter for quantitative real-time monitoring of calpain activity *in vivo*. We demonstrated by the investigation (under several conditions in skeletal muscle and by crossing the CAFI mice with a model of muscular dystrophy) that the fluorescent signals could readily be exploited in physiological and pathological studies in living mice. We provided through these analyses new insights on calpain physiology.

Interestingly, we observed a small decrease in the activity of calpains in the two atrophic conditions used or following exercise. It has been reported that calpain gene expression was stimulated in those situations (24, 29–31). In muscle atrophy, ubiquitous calpains are supposed to initiate breakdown of myofibrillar proteins for their subsequent degradation by the proteasome (32–34). Yet, the different proteolytic systems seem to participate in atrophy to different extents, depending on the conditions initiating protein breakdown (35, 36). Similarly, calpains are thought to contribute to the enhanced rate of muscle protein degradation and to promote adaptations in muscle following exercise (37–39). However, a recent report showed the absence of calpain autolysis (an event associated with their activation) after exercise in human (40). The results obtained with the CAFI mice were intermediate, confirming a calpain activity that is limited and clearly not massive under the tested situations. It is possible that this small level of detected activity is partly due to some limitations in our system. For example, the signal can be diluted throughout all the fibers,

considering that the reporter can freely move in the fibers, limiting the visualization of local activity. Furthermore, because the half-life of GFP is known to be 26 h (41), we could not detect a transient calpain activity that occurred several days before the day of observation.

We did detect substantial activity in other situations. First, we observed a high level of activity associated with structural damages of fibers following exercise. Several elements are consistent with the hypothesis that this activity corresponds to repair events rather than aberrant activity. Architecture disorganization without activation was also observed (Fig. 6*C*), suggesting that ubiquitous calpains are not at the origin of this phenomenon and that their activation is therefore secondary to the event. A decrease in FRET_{eff} was observed on the most preserved side of the fiber, which tends to prove that calpain activation was not in this case the consequence of a massive entry of Ca²⁺ with the disrupted membrane. In fact, the plugs that are observed could correspond to a kind of protection mechanism, possibly initiated to prevent complete loss of the fiber. Consistent with the literature (42, 43), those anomalies tend to disappear after several bouts of exercise (data not shown). Considering the time of the appearance of the observed activity, we would like to suggest that calpains could participate in the adaptive remodeling of the sarcomere to render the muscle less vulnerable to further exercise. This action can be put in parallel with the positive involvement of calpains in dendritic remodeling following neuronal injury (44). Second, results from CAFI muscle in the regenerative steps following notexin injection corroborate in a physiological environment what has been described in cultured muscle cell differentiation (45–50). Indeed, following destruction of the fibers, regeneration occurs and involves proliferation, migration, and then fusion of the satellite cells to form new myotubes. Results from previous investigations indicate that calpains play an important role in cytoskeletal reorganization that is requisite for myoblast migration and fusion (46, 51, 52). Altogether and in accordance with the cytoskeletal nature of many known calpain substrates, the observations made in these situations reinforce the idea that one of the physiological functions of calpains involves specific cleavage to prepare for cytoskeletal remodeling.

Beside these physiological functions, we observed calpain activity that could be considered as detrimental and pathological. (i) Following notexin administration, myofibers undergo necrosis secondary to tears created in the membranes by the toxin (53). It is therefore not surprising to see a calpain activation during the early stage as membrane disruptions should lead to a massive Ca²⁺ entry. (ii) Calpains are one of the main effectors in hypoxic/ischemic injury to the brain, liver, heart, and kidney (5, 54, 55). Our results represent the first indication that calpains are similarly activated in skeletal muscle during ischemia. (iii) Previous reports showed that calpain activation occurred in *mdx* muscle through membrane leakiness (2, 56, 57). The level of activity of calpains in the SARCAFI model suggests that deficiency in α -sarcoglycan involves a similar phenomenon. Therefore, calpain activation seems to constitute a common pathophysiological mechanism of muscular dystrophies in the context of DGC deficiency.

Our experiments show that the increase of calpain activity in ischemia is quite important, rapid, and homogeneous. Furthermore, the muscle is easily accessible for experimentation and is highly irrigated. Therefore, we believe that ischemia in skeletal muscle of CAFI mice constitutes a very good model in which to evaluate *in vivo* the potential of calpain inhibitors. In the same way, the SARCAFI model, which is to our knowledge the first report of a breeding between a reporter mouse and a pathological strain, represents another model to test calpain inhibitors in a pathological context.

Overall, we have engineered mice suitable for *in vivo* imaging of calpain activity and that can be exploited as tools to address various issues regarding calpain activity at physiological levels in disease states and for therapeutic evaluation. The CAFI mouse could be of significant value to assess the relevance of experimental models of human disorders known to involve inappropriate calpain activation. As they include spinal cord injury, stroke, cardiac infraction, and neurodegenerative diseases, they represent a significant load in terms of public health. The model would also provide more accurate methods of measuring pharmacodynamics and toxicity in the preclinical development of calpain inhibitors for these disorders.

Acknowledgments—We thank the *in vivo* department of Genethon, especially X. Broudeur, M. Durand, L. Van Wittenberg, L. Arandel, and I. Adamski for their invaluable help. We are grateful to E. Baudoin and Dr. N. Daniele for critical reading of the manuscript and Dr. J. Davoust for helpful advice. We thank Kevin P. Campbell from the Howard Hughes Medical Institute (Iowa City, IA) for providing us with *Sgca*-null mice.

REFERENCES

- Goll, D. E., Thompson, V. F., Li, H., Wei, W., and Cong, J. (2003) *Physiol. Rev.* **83**, 731–801
- Spencer, M. J., Croall, D. E., and Tidball, J. G. (1995) *J. Biol. Chem.* **270**, 10909–10914
- Nixon, R. A. (2003) *Ageing Res. Rev.* **2**, 407–418
- Tidball, J. G., and Spencer, M. J. (2000) *Int. J. Biochem. Cell Biol.* **32**, 1–5
- Vanderklish, P. W., and Bahr, B. A. (2000) *Int. J. Exp. Pathol.* **81**, 323–339
- Liu, X., Van Vleet, T., and Schnellmann, R. G. (2004) *Annu. Rev. Pharmacol. Toxicol.* **44**, 349–370
- Allen, D. G., Whitehead, N. P., and Yeung, E. W. (2005) *J. Physiol.* **567**, 723–735
- Du, S., Rubin, A., Klepper, S., Barrett, C., Kim, Y. C., Rhim, H. W., Lee, E. B., Park, C. W., Markelonis, G. J., and Oh, T. H. (1999) *Exp. Neurol.* **157**, 96–105
- Tsuji, T., Ohga, Y., Yoshikawa, Y., Sakata, S., Abe, T., Tabayashi, N., Kobayashi, S., Kohzaki, H., Yoshida, K. I., Suga, H., Kitamura, S., Taniguchi, S., and Takaki, M. (2001) *Am. J. Physiol. Heart Circ. Physiol.* **281**, H1286–H1294
- Wang, K. K., and Yuen, P. W. (1994) *Trends Pharmacol. Sci.* **15**, 412–419
- Ray, S. K., and Banik, N. L. (2003) *Curr. Drug Targets CNS Neurol. Disord.* **2**, 173–189
- Hayes, R. L., Wang, K. K., Kampfl, A., Posmantur, R. M., Newcomb, J. K., and Clifton, G. L. (1998) *Drug News Perspect.* **11**, 215–222
- Gafni, J., Hermel, E., Young, J. E., Wellington, C. L., Hayden, M. R., and Ellerby, L. M. (2004) *J. Biol. Chem.* **279**, 20211–20220
- Stockholm, D., Bartoli, M., Sillon, G., Bourg, N., Davoust, J., and Richard, I. (2005) *J. Mol. Biol.* **346**, 215–222
- Vanderklish, P. W., Krushel, L. A., Holst, B. H., Gally, J. A., Crossin, K. L., and Edelman, G. M. (2000) *Proc. Natl. Acad. Sci. U. S. A.* **97**, 2253–2258
- Duclos, F., Straub, V., Moore, S. A., Venzke, D. P., Hrstka, R. F., Crosbie, R. H., Durbeej, M., Lebakken, C. S., Ettinger, A. J., van der Meulen, J., Holt, K. H., Lim, L. E., Sanes, J. R., Davidson, B. L., Faulkner, J. A., Williamson, R., and Campbell, K. P. (1998) *J. Cell Biol.* **142**, 1461–1471
- Ikawa, M., Kominami, K., Yoshimura, Y., Tanaka, K., Nishimune, Y., and Okabe, M. (1995) *Dev. Growth Differ.* **37**, 455–459
- Stockholm, D., Herasse, M., Marchand, S., Praud, C., Roudaut, C., Richard, I., Sebille, A., and Beckmann, J. S. (2001) *Am. J. Physiol. Cell Physiol.* **280**, C1561–1569
- Gordon, G. W., Berry, G., Liang, X. H., Levine, B., and Herman, B. (1998) *Biophys. J.* **74**, 2702–2713
- Gil-Parrado, S., Assfalg-Machleidt, I., Fiorino, F., Deluca, D., Pfeiler, D., Schaschke, N., Moroder, L., and Machleidt, W. (2003) *Biol. Chem.* **384**, 395–402
- Belcastro, A. N., Albisser, T. A., and Littlejohn, B. (1996) *Can. J. Appl. Physiol.* **21**, 328–346
- Baker, J. H., and Margolis, R. N. (1987) *Muscle Nerve* **10**, 34–40
- Feasson, L., Stockholm, D., Freyssenet, D., Richard, I., Duguez, S., Beckmann, J. S., and Denis, C. (2002) *J. Physiol.* **543**, 297–306
- Ilian, M. A., and Forsberg, N. E. (1992) *Biochem. J.* **287**, 163–171
- Moraczewski, J., Piekarska, E., Zimowska, M., and Sobolewska, M. (1996) *Acta Biochim. Pol.* **43**, 693–700
- Sultan, K. R., Dittrich, B. T., and Pette, D. (2000) *Am. J. Physiol. Cell Physiol.* **279**, C639–647
- French, J. P., Quindry, J. C., Falk, D. J., Staib, J. L., Lee, Y., Wang, K. K., and Powers, S. K. (2006) *Am. J. Physiol. Heart Circ. Physiol.* **290**, H128–H136
- Iwata, Y., Katanosaka, Y., Shijun, Z., Kobayashi, Y., Hanada, H., Shigekawa, M., and Wakabayashi, S. (2005) *Biochem. Pharmacol.* **70**, 740–751
- Nakashima, K., Komatsu, T., Yamazaki, M., and Abe, H. (2005) *J. Nutr. Sci. Vitaminol. (Tokyo)* **51**, 248–253
- Kumamoto, T., Kleese, W. C., Cong, J. Y., Goll, D. E., Pierce, P. R., and Allen, R. E. (1992) *Anat. Rec.* **232**, 60–77
- Elce, J. S., Hasspieler, R., and Boegman, R. J. (1983) *Exp. Neurol.* **81**, 320–329
- Huang, J., and Forsberg, N. E. (1998) *Proc. Natl. Acad. Sci. U. S. A.* **95**, 12100–12105
- Jackman, R. W., and Kandarian, S. C. (2004) *Am. J. Physiol. Cell Physiol.* **287**, C834–C843
- Bartoli, M., and Richard, I. (2005) *Int. J. Biochem. Cell Biol.* **37**, 2115–2133
- Furuno, K., Goodman, M. N., and Goldberg, A. L. (1990) *J. Biol. Chem.* **265**, 8550–8557
- Tischler, M. E., Rosenberg, S., Satarug, S., Henriksen, E. J., Kirby, C. R., Tome, M., and Chase, P. (1990) *Metabolism* **39**, 756–763
- Arthur, G. D., Booker, T. S., and Belcastro, A. N. (1999) *Can. J. Physiol. Pharmacol.* **77**, 42–47
- Ertbjerg, P., Henckel, P., Karlsson, A., Larsen, L. M., and Moller, A. J. (1999) *J. Anim. Sci.* **77**, 2428–2436
- Belcastro, A. N. (1993) *J. Appl. Physiol.* **74**, 1381–1386
- Murphy, R. M., Snow, R. J., and Lamb, G. D. (2006) *Am. J. Physiol. Cell Physiol.* **290**, C116–C122
- Corish, P., and Tyler-Smith, C. (1999) *Protein Eng.* **12**, 1035–1040
- Stupka, N., Tarnopolsky, M. A., Yardley, N. J., and Phillips, S. M. (2001) *J. Appl. Physiol.* **91**, 1669–1678
- McHugh, M. P. (2003) *Scand J. Med. Sci. Sports* **13**, 88–97
- Faddis, B. T., Hasbani, M. J., and Goldberg, M. P. (1997) *J. Neurosci.* **17**, 951–959
- Raynaud, F., Carnac, G., Marcilhac, A., and Benyamin, Y. (2004) *Exp. Cell Res.* **298**, 48–57
- Dedieu, S., Poussard, S., Mazeret, G., Grise, F., Dargelos, E., Cottin, P., and Brustis, J. J. (2004) *Exp. Cell Res.* **292**, 187–200
- Moraczewski, J., Piekarska, E., Bonavaud, S., Wosinska, K., Chazaud, B., and Barlovatz-Meimon, G. (1996) *CR Acad. Sci. III* **319**, 681–686
- Kumar, A., Shafiq, S., Wadgaonkar, R., and Stracher, A. (1992) *Cell Mol. Biol. (Noisy-le-grand)* **38**, 687–691
- Barnoy, S., Maki, M., and Kosower, N. S. (2005) *Biochem. Biophys. Res. Commun.* **332**, 697–701
- Zimowska, M., Constantin, B., Papy-Garcia, D., Raymond, G., Cognard,

Calpain Activity followed by FRET in Model Mice

- C., Caruelle, J. P., Moraczewski, J., and Martelly, I. (2005) *J. Cell. Physiol.* **205**, 237–245
51. Kwak, K. B., Chung, S. S., Kim, O. M., Kang, M. S., Ha, D. B., and Chung, C. H. (1993) *Biochim. Biophys. Acta* **1175**, 243–249
52. Barnoy, S., Glaser, T., and Kosower, N. S. (1998) *Biochim. Biophys. Acta* **1402**, 52–60
53. Harris, J. B., and Johnson, M. A. (1978) *Clin. Exp. Pharmacol Physiol.* **5**, 587–600
54. Kanimatsu, M., Tada, T., Narita, Y., Ozaki, Y., Liu, Z. Q., Shearer, T. R., and Sasaki, M. (1999) *Cardiovasc Pathol.* **8**, 7–15
55. Zalewska, T. (1996) *Folia Neuropathol.* **34**, 121–127
56. Turner, P. R., Schultz, R., Ganguly, B., and Steinhardt, R. A. (1993) *J. Membr. Biol.* **133**, 243–251
57. Gillis, J. M. (1999) *J. Muscle Res. Cell Motil.* **20**, 605–625